Compliant Suction Gripper With Seamless Deployment and Retraction for Robust Picking Against Depth and Tilt Errors

Yuna Yoo, Jaemin Eom, MinJo Park, and Kyu-Jin Cho, *Member, IEEE*

***Abstract*—Applying suction grippers in unstructured environments is a challenging task because of depth and tilt errors in vision systems, requiring additional costs in elaborate sensing and control. To reduce additional costs, suction grippers with compliant bodies or mechanisms have been proposed; however, their bulkiness and limited allowable error hinder their use in complex environments with large errors. Here, we propose a compact suction gripper that can pick objects over a wide range of distances and tilt angles without elaborate sensing and control. The spring-inserted gripper body deploys and conforms to distant and tilted objects until the suction cup completely seals with the object and retracts immediately after, while holding the object. This seamless deployment and retraction is enabled by connecting the gripper body and suction cup to the same vacuum source, which couples the vacuum picking and retraction of the gripper body. Experimental results validated that the proposed gripper can pick objects within 79 mm, which is 1.4 times the initial length, and can pick objects with tilt angles up to 60°. The feasibility of the gripper was verified by demonstrations, including picking objects of different heights from the same picking height and the bin picking of transparent objects.**

***Index Terms*—Mechanism design, soft robot materials and design, unstructured environment, physical intelligence, suction gripper.**

I. Introduction

SUCTION grippers have been widely used for pick-and-place tasks due to their robustness, versatility, and high operating speed [1], [2]. With growing demand for automatic picking systems in unstructured environments, recent studies on suction grippers focus not only on picking in highly-structured environments such as factory lines but also on picking in cluttered or unstructured real-world environments including bin picking [3] and warehouse picking [4].

Manuscript received 8 September 2022; accepted 10 January 2023. Date of publication 23 January 2023; date of current version 31 January 2023. This letter was recommended for publication by Associate Editor H. Su and Editor Y.-L. Park upon evaluation of the reviewers' comments. This work was supported in part by The Ministry of Trade, Industry and Energy (MOTIE), Korea, under Grant 20008908 and in part by the National Research Foundation of Korea (NRF) funded by Korean Government (MSIT) under Grant NRF-2016R1A5A1938472. *(Yuna Yoo and Jaemin Eom contributed equally to this work.) (Corresponding author: Kyu-Jin Cho.)*

The authors are with the Biorobotics Laboratory, Soft Robotics Research Center, Institute of Advanced Machines and Design, Department of Mechanical Engineering, Institute of Engineering, Seoul National University, Seoul 08826, Korea (e-mail: yunayoo@snu.ac.kr; jaemineom@snu.ac.kr; mjpark1995@gmail.com; kjcho@snu.ac.kr).

This letter has supplementary downloadable material available at https://doi.org/10.1109/LRA.2023.3238903, provided by the authors.

Digital Object Identifier 10.1109/LRA.2023.3238903

While identifying the exact location of an object is important for reliable picking, recognizing the accurate distance and tilt angle between the suction gripper and object remains a challenge when picking in unstructured environments. The errors in the depth and tilt data obtained from vision systems can be up to tens of centimeters and degrees, respectively, due to factors such as transparency [5], [6], reflective or dark surfaces [7], lack of texture [8], background illumination [9], or occlusion by the gripper [10]. These depth and tilt errors lower the reliability of picking, as approaching at an improper distance or angle results in the failure of picking, or damages the object [11], [12]. Studies have been conducted to solve this reliability problem using computational algorithms, machine learning [13], [14], or by using vision systems in combination with tactile sensors to measure and correct the depth and tilt errors [10], [15]. However, additional costs are incurred for additional sensor and control systems or complex algorithms.

To reduce vision, sensing, or control costs, grippers that can offload system complexities onto intelligent mechanical designs based on 'physical intelligence' have been developed [16], [17]. Grippers with physical intelligence can improve the reliability of picking by conforming to various shapes and sizes of objects [18], [19] or misaligned objects [18], [20], [21] through the compliance of the end effector. To alleviate the depth errors with physical intelligence, vacuum cylinders can be used [22], which operate by pushing the suction cup forward and pulling it back when a suction seal is formed. However, vacuum cylinders cannot compensate for tilt errors due to the rigidity of the cylinders, and they occupy several times the space required for their stroke when at rest, rendering the system bulky. On the other hand, bellows suction cups can mitigate both depth and tilt errors, because their bellows-shaped body conforms to the object by folding in response to object contact [12], [23]. However, the allowable depth error, which is determined by the length of the bellows-shaped body, is difficult to be designed for more than a few centimeters due to the risk of uncontracted bellows-shaped body colliding with environment.

In this letter, we developed a compliant deployable suction gripper with a compact structure that enables reliable picking against a wide range of depth and tilt errors, without additional sensing and control. The proposed gripper longitudinally deploys its compliant body while conforming to a distant or tilted object, and retracts while holding the object as soon as the suction cup seals against the object as shown in Fig. 1. The

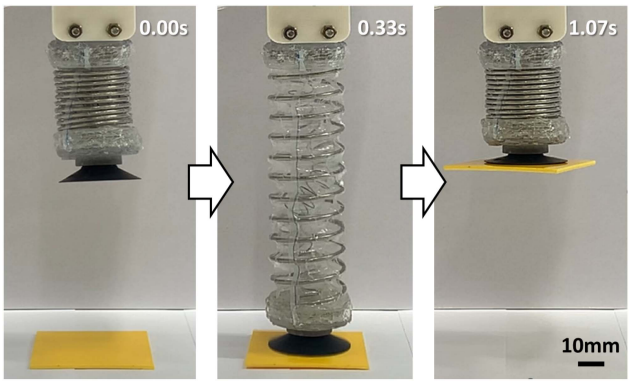

Fig. 1. Proposed suction gripper picking up a distant object through seamless deployment and retraction.

gripper remains contracted after releasing the object to be in a compact form when not in operation. There are two key enabling technologies for gripper motion. The deployable and bendable spring-inserted gripper body enables conforming to distant and tilted objects. Connecting the gripper body and suction cup to the same vacuum source enables seamless deployment and retraction by coupling the vacuum picking and retraction of the gripper body. With these enabling technologies, the proposed gripper compensates for depth and tilt errors up to 79 mm and 60° which are six and two times larger, respectively, compared to the bellows suction cup of similar length to the proposed gripper. The proposed gripper picks up objects with maximum deployment and retraction speed of 3.23 m/s and 1.51 m/s, repectively, and picks up objects weighing up to 4400 g, also having robustness verified by 1000 cycles of repeatability test. The picking ability of the proposed gripper against depth and tilt errors was verified by demonstrations, including picking objects with different heights from the same picking height and bin picking of transparent objects. Furthermore, the gripper was applied to depalletizing tasks, and a gripper with extended stroke of 140 mm was applied to pick objects in narrow, deep spaces, which cannot be reached by manipulators. Finally, the proposed gripper was applied to catch a falling balloon using its fast speed, demonstrating the possibility of dynamic grasping. The limitation of the proposed gripper is that it can only pick up objects with flat surface or curved surface with low curvature since we used a flat suction cup. However, as our gripper is designed to be able to replace the suction cup, target-specific suction cups can be used if necessary to overcome this limitation.

The rest of this letter is organized as follows. Section II presents the design and fabrication method. Section III presents the theoretical modeling of the gripper. Section IV presents the experimental verification of the performance of the gripper. Section V presents the demonstrations of the proposed gripper. Section VI concludes the letter.

II. Mechanical Design and Fabrication

A. Overall Structure and Picking Strategy

To pick up objects against depth and tilt errors without sensing, the proposed gripper was designed to deploy longitudinally and retract while holding the object as soon as the gripper seals against the object. The key design requirement for this gripper operation was a system that enables seamless deployment and retraction without sensors, which was facilitated by structurally embedding the operation sequence into the proposed gripper and pneumatic circuit.

As shown in Fig. 2(a), the proposed gripper comprised two concentric cylindrical chambers, where the outer and inner chambers are termed as the spring-inserted gripper body and spring-inserted air tube, respectively. The gripper body retracts and deploys when negative pressure is applied or released, and the air tube provides the airway to the suction cup. The pneumatic circuit included a vacuum pump (N035AN.18, KNF Neuberger Inc.), a 3-way solenoid valve (UV307-4LL, Shinyeong Mechatronics Co., Ltd.), and urethane pneumatic hoses with a diameter of 6 mm. In the circuit, the gripper body was directly connected to the vacuum pump and the air tube was connected to the pump or atmosphere through the 3-way valve.

The picking strategy utilizing a pneumatic circuit and deployable gripper is illustrated in Fig. 2(b). First, in the 'ready-to-pick' stage, the valve connects the suction cup and the atmosphere. The gripper body becomes a closed space connected to the vacuum pump; therefore, the gripper body is vacuumized by the pump and contracted. The gripper moves to the picking stage when the valve switches and connects the suction cup and gripper body. Thereafter, the gripper body is connected to the atmosphere through the suction cup, so the sealing is released and the body deploys. When the suction cup contacts and seals with the object, the entire space inside the gripper is vacuumized, and the gripper body retracts immediately, while the suction cup holds the object. The manipulator then moves the gripper to the desired position. Finally, when the valve is switched to connect the suction cup to the atmosphere, the suction cup releases the object while the gripper body remains contracted, then the gripper returns to the ready-to-pick state. Connecting the suction cup and gripper body to the same vacuum source throughout the picking stage enables seamless deployment and retraction without sensors, and disconnecting the suction cup and gripper body when releasing the object enables the gripper to be contracted when not in use.

B. Gripper Design

The gripper body was designed as a compressible spring enclosed in a cylindrical LDPE film for the following reasons: First, the gripper can be deployed at a high speed due to the restoring force of the spring. Second, the gripper can conform to tilted objects during deployment. Finally, the radially incompressible characteristics of the spring allow the gripper to retract effectively in the longitudinal direction.

The spring-inserted air tube which connects the suction cup and valve was built inside the gripper body with a compressible spring encased in a cylindrical LDPE film with the same structure as the gripper body. The radial incompressibility of the spring prevents airway clogging during the retraction. To prevent the air tube from affecting the movement of the gripper body, the wire diameter of the spring in the air tube was determined to be 0.5 mm, which is the thinnest to be manufactured.

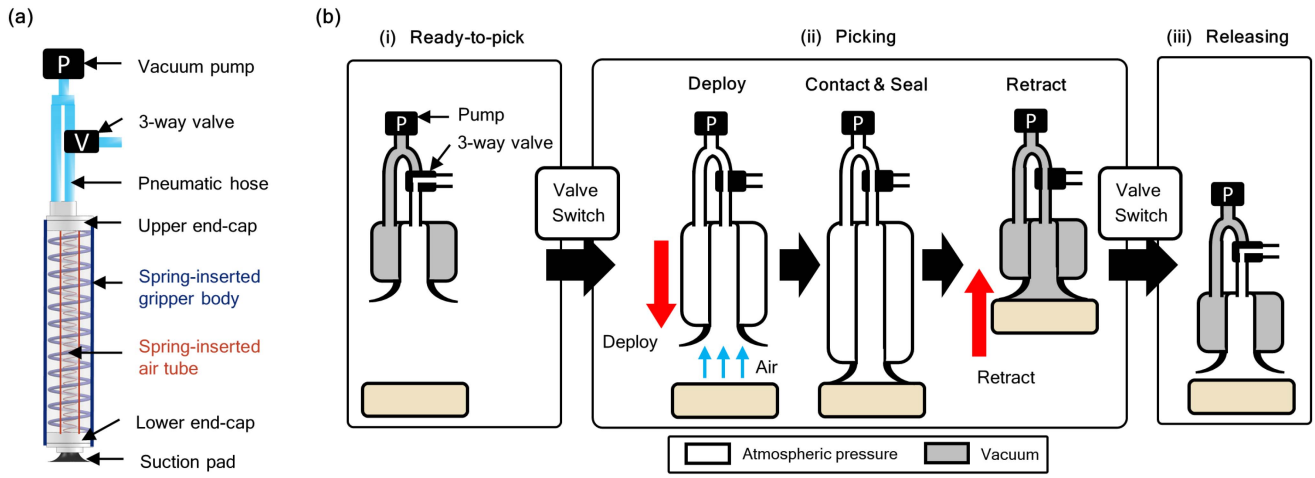

Fig. 2. Design and strategy of the proposed gripper. (a) Overall structure of the proposed gripper system: the system comprises a gripper containing two concentric chambers and a pneumatic circuit connected to the gripper. (b) Picking strategy of the gripper: (i) the gripper is contracted in the ready-to-pick stage; (ii) the gripper moves on to the picking stage when the valve switches, and seamlessly deploys and retracts to pick up an object.

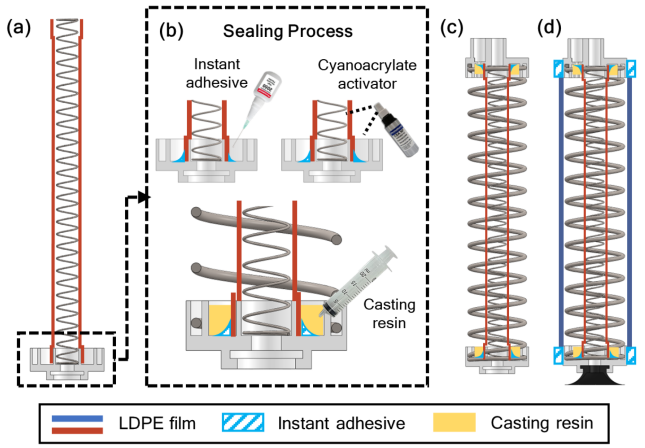

Fig. 3. Fabrication process of the proposed gripper: (a) Assembling the inner spring, inner LDPE film, and the lower end-cap; (b) sealing process using instant adhesive and casting resin; (c) assembling the outer spring and the upper end-cap; (d) sealing the outer LDPE film and plugging in the suction cup.

C. Gripper Fabrication

The upper and lower end-caps were 3D printed using OBJET30 Dental Prime (Stratasys Ltd.). The outer and inner LDPE films are fabricated by heat-pressing two 60 μm thick planar LDPE sheets at 230 °C. Fig. 3 shows the overall fabrication process of the gripper. First, the inner spring was inserted into the inner LDPE film. The inner LDPE film and the lower end-cap were sealed with instant adhesive (Permabond 2050, Permabond Engineering Adhesives Ltd.), and a cyanoacrylate activator (Permabond CSA-NF, Permabond Engineering Adhesives Ltd.) was used to promote a faster cure. For additional sealing, the casting resin (TASK 2, Smooth-on Inc.) was poured into the end-caps and cured at room temperature for an hour. Subsequently, the outer spring was inserted, and the assembled parts were covered and sealed with an upper end-cap. The assembled parts were placed in the outer LDPE film, which was sealed with the upper and lower end-caps using the same sealing process. Finally, the suction cup was placed at the connection part of the lower end-cap.

III. Modeling

To analyze the picking ability of the proposed gripper according to the depth error, two analytical models were devised: the picking distance range from objects for successful picking and the maximum picking force according to the distance from the object.

A. Picking Distance Range

To analyze the allowable depth error, that is, the picking distance range for the gripper to successfully pick up an object, the maximum and minimum distances were modeled. The distance was defined as the distance between the upper surface of the gripper and the upper surface of the object.

The minimum distance (d_{min}) is the maximum contracted length of the gripper. Two cases of minimum distance exist: the gripper contracts until the restoring force of the spring and contracting force caused by the vacuum are in equilibrium (1); the gripper contracts completely when the maximum restoring force of the spring is weaker than the contracting force (2).

$$d_{\text{min}} = L - \frac{P_{\text{atm}} A_b}{k_b} + h_{\text{endcap}} + h_{\text{suction}} \tag{1}$$

$$d_{\text{min}} = N_t t + 2(N_t - 1)t_{\text{film}} + h_{\text{endcap}} + h_{\text{suction}} \tag{2}$$

where h_{endcap} is the sum of the heights of the two end-caps, h_{suction} is the height of the suction cup, t is the wire diameter of the spring, N_t is the total number of coils, and t_{film} is the LDPE film thickness.

The maximum distance (d_{max}) was defined as the fully deployed length of the gripper. Fig. 4 shows the schematic of the fully deployed gripper at the steady state. A pressure drop occurs from P_{atm} to P_b along the spring-inserted air tube and polyurethane (PU) tube ② due to the airflow, whereas the

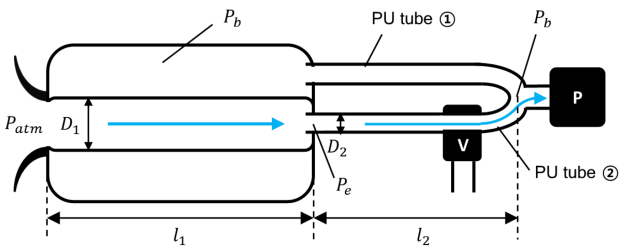

Fig. 4. Schematic of the gripper system at the fully-deployed steady-state.

pressure inside the gripper body and the PU tube ① are constant with P_b because there is no airflow along this path. The fully deployed length is smaller than the initial length, L, due to the contraction caused by the pressure difference (ΔP) between the inside (P_b) and outside (P_{atm}) of the gripper body.

The airflow can be assumed incompressible because the maximum velocity in the proposed system is 18.6 m/s, which is smaller than Mach 0.3 (p. 175, [24]). Then, assuming that the effects of gravity and minor losses due to the elbow, fittings, and valves are negligible, the pressure drop due to airflow is derived as follows (Equation (6.10) in [24]):

$$\frac{\Delta P}{\rho g} = h_f = \frac{8 f L_t Q^2}{\pi^2 g D^5} \tag{3}$$

where ρ is density of air, h_f is head loss, f is friction factor of the air tube, L_t is the length of tube, Q is the flow rate of air, and D is the tube diameter. The pressure drop along the spring-inserted air tube was ignored, because it was approximately 200 times smaller than the pressure drop along the PU tube based on (3), due to the difference between the diameter and length. Because the Reynolds number for the slowest airflow in the tube is 4453, the airflow is turbulent in all Q ranges (4-14 L/min). In turbulent flow, the friction factor is obtained as follows (Equation (6.49) in [24]):

$$\frac{1}{f^{1/2}} \approx -1.8 \log \left[\frac{6.9}{\text{Re}} + \left(\frac{\epsilon / D_2}{3.7} \right)^{1.11} \right], \left(\text{Re} = \frac{4 \rho Q}{\mu \pi D_2} \right) \tag{4}$$

where V is airflow speed, μ is the specific gravity of air, and ϵ is the roughness value of the tube. By substituting (4) into (3), ΔP is obtained and $d_{\max}$ can be derived as follows:

$$d_{\max} = L - \frac{\Delta P A_b}{k_b} + h_{\text{endcap}} + h_{\text{suction}} \tag{5}$$

B. Maximum Picking Force

The maximum picking force exerted by the gripper according to the distance from the object was analyzed. The configuration and free-body diagram of the gripper body and suction cup when it is in contact with the object are shown in Fig. 5(a) and (b). We assumed that the weights of the spring and other components of the gripper were negligible throughout the picking process. In this paper, the force applied by the gripper body to lift the object is called the lifting force F_b, and that applied by the suction cup on the object is called the holding force F_s. The lifting and holding forces satisfy the following equation and inequality:

$$F_b = (P_{\text{atm}} - P_b) A_b - k_b (L - l) \tag{6}$$

$$F_s \leq (P_{\text{atm}} - P_s) A_s \tag{7}$$

where P_{atm} is the atmospheric pressure; P_b, P_s, A_b, and A_s are the internal pressure and effective area of the gripper body and suction cup, respectively; k_b is the coefficient of spring; and L and l are the initial and current lengths of the spring, respectively.

For the gripper to lift an object without dropping it, the following condition should be satisfied:

$$\min(F_{b,\max}, F_{s,\max}) \geq mg \tag{8}$$

where m is the weight of the object, $F_{s,\max}$ and $F_{b,\max}$ are the forces when the internal pressure is closest to the vacuum. This is because the gripper cannot retract or can drop the object when the weight of the object exceeds the minimum of $F_{s,\max}$ and $F_{b,\max}$, which is therefore the maximum picking force of the gripper.

$F_{s,\max}$ and $F_{b,\max}$ have linear relationship with the effective areas of the suction cup and gripper body, respectively, as expressed in (6) and (7). The effective area of the suction cup is constant regardless of the distance from the object, however, that of the gripper body decreases as the gripper approaches the object. This is because the LDPE film slacks and sticks to the upper and lower end-caps during gripper retraction (Fig. 5(c)) [25]. Therefore, to analyze the maximum picking force, the effective area of the gripper body was modeled according to the distance between the suction cup and object.

The effective area model was based on one fundamental condition called the contact condition: the film contacted tangentially to the upper and lower end-caps and spring. According to the initial length of the film (l_1), there are three film configurations (Fig. 5(d)): non-contact, single contact, and double contact. The non-contact state indicates that the film and lower end-cap lacked contact; the single contact state means that the film and lower end-cap are in contact; and the double contact state means that the film completely wraps around the spring and they are in contact with each other. The boundary value of l_1 between states is derived as follows:

$$l_{n,s} = \left(\left(\frac{{l'_1}^2 + t + 1}{2 l'_1} \right) \left(\theta_{n,s} + \frac{\pi}{2} \right) \right) + \frac{t \theta_{n.s}}{2} \tag{9}$$

$$l_{s,d} = \frac{1}{2} \left(t \left(\theta_{s,d} + 1 + \sin \left(\theta_{s,d} - \frac{\pi}{2} \right) \right) + l'_1 \left(\theta_{s,d} + \frac{\pi}{2} + \sin \left(\theta_{s,d} - \frac{\pi}{2} \right) \right) + 1 \right) \tag{10}$$

where $l_{n,s}$ and $l_{s,d}$ are the boundary values between the non-contact and single contact states, and between the single and the double contact states, respectively; l'_1 is the distance between the cross section of the spring and lower end-cap; $\theta_{n,s}$ and $\theta_{s,d}$ are the angles at which the film wraps around the spring and are derived as follows:

$$\theta_{n,s} = \cos^{-1} \left(\frac{(t/2) + 1}{\left(({l'_1}^2 + t + 1) / 2 l'_1 \right) + (t/2)} \right) \tag{11}$$

$$\theta_{s,d} = \pi - \sin^{-1} \left(\frac{l'_1}{l'_1 + t} \right) \tag{12}$$

For the single and double contact states, the length of the film in contact with the lower end-cap (d) is derived through (13) and

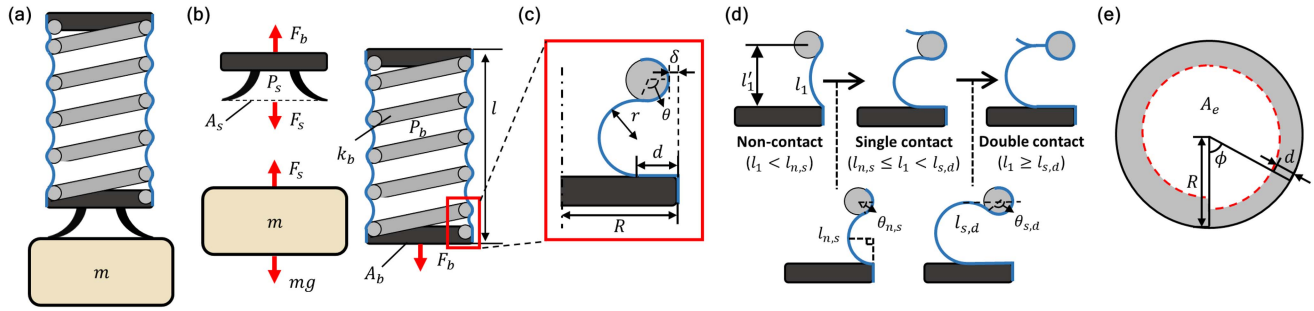

Fig. 5. (a) Configuration of the gripper body when the suction cup is in contact with an object. (b) Free body diagram of the gripper body, suction cup, and the object. (c) Configuration of the film that contacts the lower end-cap as the gripper body retracts. (d) Three states of film configurations during retraction: non-contact, single contact, and double contact states. (e) Top-view of lower end-cap while film contacts to the end-cap: the gray area indicates the contact area.

TABLE I
SPRING PARAMETERS

	Outer Spring				Inner Spring
Free Length (L, mm)	150				150
Radius (R_s, mm)	15				5
Pitch (p, mm)	11.5				5.36
Wire Diameter (t, mm)	1.4	1.6	1.8	2.0	0.5
Spring Constant (k_b, N/m)	125	198	326	522	22.3

(14), respectively, as follows:

$$\begin{cases} r + \left(\left(r + \frac{t}{2}\right)\sin\theta\right) - l_1' = 0 \\ r\left(\theta + \frac{\pi}{2}\right) + \frac{t}{2}\theta + d - l_1 = 0 \\ \delta + \frac{t}{2} - \left(r + \frac{t}{2}\right)\cos\theta - d = 0 \end{cases} \tag{13}$$

$$d = \frac{1}{2}\left(l_1 - \frac{\pi}{2}l_1' - \left(\frac{\pi}{2} - 1\right)t + \delta\right) \tag{14}$$

where r is the radius of the non-contact part of the film, θ is the wrapped angle by film, and δ is the difference between the radius of the outer spring and the end-cap.

Because the spring is spirally formed, l_1, l_1', and d vary along the circumference of the end-cap (Fig. 5(e)). Therefore, the effective area is obtained as follow:

$$A_e = \int_0^{2\pi} \frac{1}{2}(R - d)^2 \, d\phi \tag{15}$$

where A_e is the effective area and R is the radius of the lower end-cap.

IV. EXPERIMENTS

A. Picking Range

The picking range comprises the picking distance and picking angle ranges, corresponding to the allowable depth and tilt error, respectively. First, the picking distance range according to the flow rate and spring constant of the gripper was measured and compared with the modeling to validate the robustness of the proposed gripper against depth error. Four grippers with different outer-spring constants, each with a wire diameter of 1.4, 1.6, 1.8, and 2.0 mm, were prepared. The other parameters of the spring, including spring constant k, are listed in Table I.

The picking distance range and deployment ratio, which were calculated by dividing the fully deployed length by the contracted length, are shown in Fig. 6. As the wire diameter of the

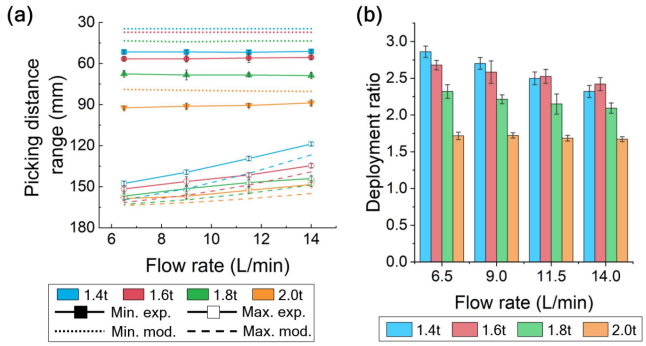

Fig. 6. Experimental verification for the picking distance range. (a) Maximum and minimum distance and (b) deployment ratio of the gripper according to the flow rate and the diameter of spring wire. Error bars represent threefold standard deviations.

spring increased, both the contracted and fully deployed lengths increased, because a thicker spring applies a larger restoring force. In addition, as the flow rate increased, the fully deployed length decreased due to the pressure drop in the pneumatic line; therefore, the deployment ratio decreased. The mean absolute percentage error (MAPE) of the maximum distance model was about 4.4 %, but the MAPE of the minimum distance model was 28.5 %. This error is because the proposed model could not consider the wrinkles of the film and the buckling of the internal spring during body contraction, which prevent the gripper body from maximally contracting.

To validate the robustness of the gripper against tilt errors, the success rate of picking up a 5 g plate lying on the tilted structure for varying distance and tilt angle values was measured (Fig. 7(a)). The distance to the object (l_{dist}) is defined as the distance between the upper surface of the gripper and the center of the contact point, and the tilt angle (θ_{tilt}) is the angle of the tilted structure from the horizontal line. The picking was repeated 10 times for each specimen varying the distance and tilt angle.

As shown in Fig. 7(b), for all four grippers, as the distance increased, failure occurred at increasingly smaller tilt angles because of the two failure modes. The first failure mode primarily occurred for grippers with small spring constants, where the suction cup could not reach the plate because of the insufficient restoring force of the gripper for conforming to the object. The

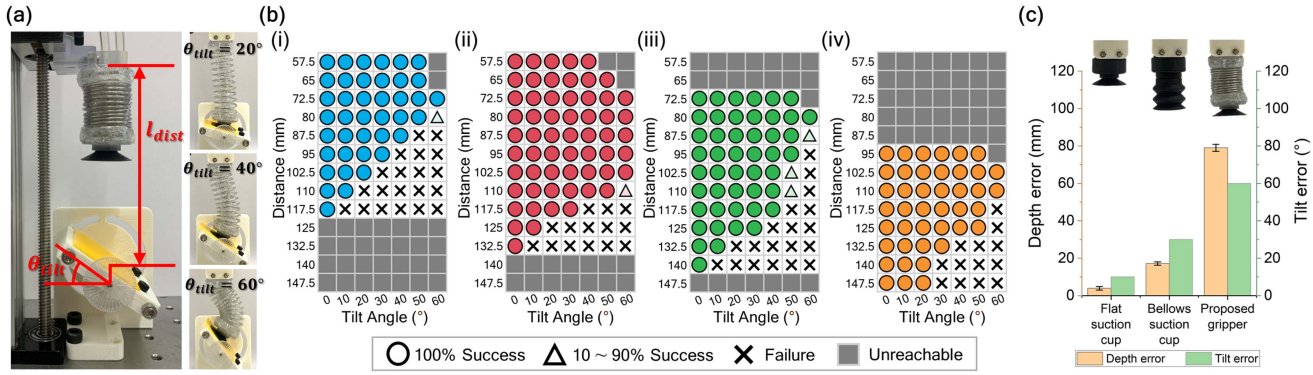

Fig. 7. Picking range experiment. (a) Experimental setup for the picking range test. (b) Success rate for picking distant and tilted object with the gripper having (i) 1.4 mm (ii) 1.6 mm (iii) 1.8 mm (iv) 2.0 mm of wire diameter. (c) Allowable depth and tilt errors of the proposed gripper compared with the flat and bellows suction cups. Error bars represent threefold standard deviations.

second failure mode, primarily occurred for grippers with large spring constants, where slip occurred because of the insufficient friction force between the suction cup and plate for stopping the rapidly deploying gripper. Consequently, the gripper of wire diameter 1.6 mm showed the widest picking range. For θ_{tilt} larger than 60°, picking failed for all grippers under the second failure mode because of insufficient normal force to generate sufficient friction.

Fig. 7(c) summarizes the picking ability against the depth and tilt errors of the proposed gripper and compares it with the flat (VFU30-N-M5M, F.TEC) and bellows (VFB30-N-18 N, F.TEC) suction cups. For these suction cups, the maximum distance was defined as the position at which the object would start to be picked up when the suction cup approached the object under negative pressure. The minimum distance was defined as the position at which the suction cup could be compressed to its maximum. The maximum tilt angle was measured by testing at each tilt angle of 10° intervals if the gripper can pick up the object when the suction cup approaches the object with negative pressure. The allowable depth and tilt errors of the gripper were about 79 mm and 60°, respectively, which are two to 26 times larger than those of the flat or bellows suction cups, verifying the applicability of the proposed gripper.

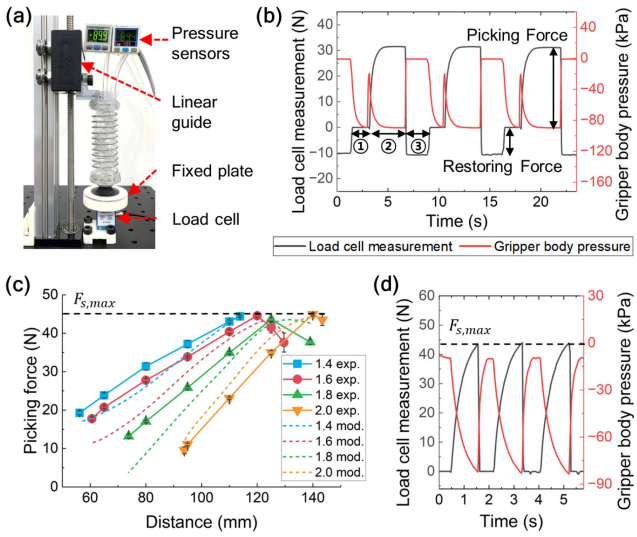

Fig. 8. Picking force experiment. (a) Experimental setup for the picking force test. (b) Raw data of the picking force experiment: the gripper is ① contracted, ② deploys and pulls the fixed plate upwards, and ③ releases it. (c) Picking force according to the distance and spring constant compared with the modeling results. Error bars represent threefold standard deviations. (d) Raw data when the suction cup falls off from the fixed plate.

B. Picking Force

The picking force was measured to determine the maximum weight of the object that the gripper could pick according to the picking distance and spring constant. Fig. 8(a) shows the experimental setup. The picking force was measured by lifting the fixed plate attached to the load cell (333FDX, KTOYO). The pressure in the suction cup and gripper body was measured using pressure sensors (ZSE30A-C6H-C, SMC), and the flow rate was fixed at 14 L/min. The picking force tests were repeated 5 times each.

Fig. 8(b) shows the pressure data of the gripper body and the force data measured by the load cell during the picking force experiment. Starting with the contracted gripper (① in Fig. 8(b)), the gripper deployed and sealed with a fixed plate, and an upward force was applied to the load cell (② in Fig. 8(b)). The picking force was measured as the maximum force in state ②.

To measure the spring constant of the compressible spring built inside the gripper, the restoring force of the spring was measured by connecting the inner and outer chambers of the gripper to the atmosphere (③ in Fig. 8(b)). The experimental and modeling results for the picking force are shown in Fig. 8(c). The picking force increases for increasing distance or decreasing spring constant, because the restoring force of the spring decreases, and the effective area of the body increases. However, the picking force cannot exceed 45 N ($F_{s,\max}$), because the suction cup falls off from the fixed plate. This situation can also be observed in the raw data in Fig. 8(d), where the picking force drops to zero as soon as it reaches $F_{s,\max}$. When the suction cup falls off from the fixed plate, the radius of the suction cup' s effective area is less than 15 mm because the suction cup cannot exert lifting force in the contact area between the object and the suction cup. This effect limits $F_{s,\max}$ to 45 N. Furthermore, increasing the

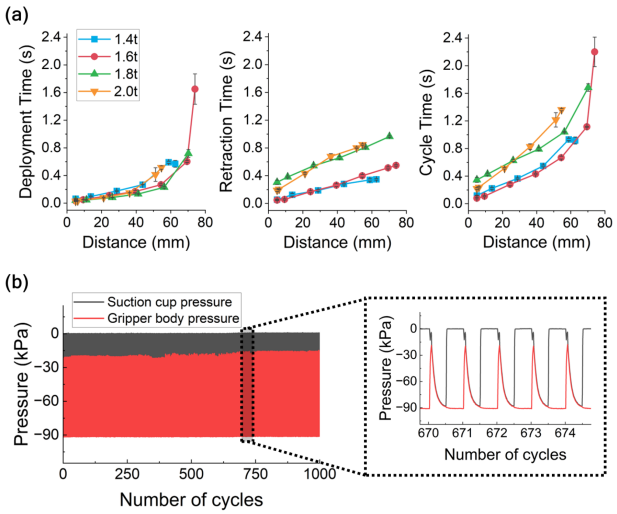

Fig. 9. (a) Cycle time experiment according to the wire diameter of spring and distance to the object. Error bars represent standard deviations. (b) Reliability test of 1000 cycles.

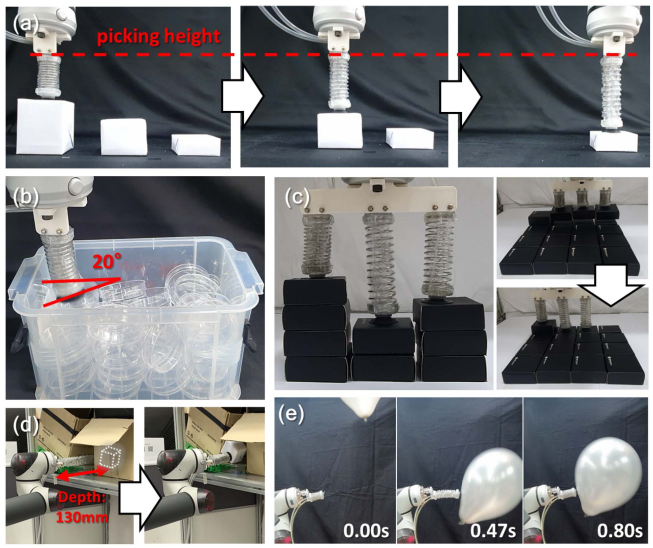

Fig. 10. Demonstrations on the proposed gripper. (a) Picking objects with different height from the same picking height. (b) Bin picking of transparent objects that cause large errors in depth sensing. (c) Solving depalletizing task by simultaneously picking objects with different heights. (d) Warehouse picking through a narrow, deep space. (e) Dynamic grasping of a falling balloon.

distance from the point where the suction cup starts to fall off results in a decrease in the picking force, because the suction cup cannot be tightly attached, and the effective area decreases. The mean absolute percentage error of the picking force model was 16.8%. A slight difference occurs due to the buckling of the inner spring or the mass of the gripper, which is not considered in the model.

C. Picking Speed

To test the picking speed, the cycle time of the proposed gripper was measured through picking video analysis while changing the distance and the outer spring wire diameter (Fig. 9(a)). The picking speed tests were repeated 5 times each. The increment of deployment time gradually increased after the gripper reached around 70 % of the gripper' s stroke. This is because friction between the LDPE film and spring, and viscoelastic force due to the deformation of the LDPE film exerts in the opposite direction of the deployment, and restoring force of the spring gradually decreases as the gripper reaches the force equilibrium point. Therefore, grippers with wire diameters of 1.6 and 1.8 mm which have longer stroke than the other two specimens had shorter deployment time. In case of retraction, grippers with wire diameters of 1.4 and 1.6 mm had shorter retraction time. These two specimens fully retract before the vacuum and restoring forces reach equilibrium due to their small restoring force. However, the other two specimens retract until the equilibrium between the vacuum and restoring force is reached, and longer time is required to converge to the force equilibrium. As a result, the gripper with a wire diameter of 1.6 mm had the shortest cycle time since it had the longest stroke, and its maximum restoring force was smaller than the vacuum force. This means that the gripper with a wire diameter of 1.6 mm showed the fastest picking speed, where the maximum deployment and retraction speed of the gripper was 3.23 m/s and 1.51 m/s, respectively.

D. Reliability and Scalability

We performed a reliability test (Fig. 9(b)) by picking and placing a thin plate of 5 g 1000 times with a gripper of wire diameter 1.6 mm. The maximum suction cup pressure changed within 4.3 % during 1000 cycles but did not affect the gripper performance. The minimum pressure inside the gripper body was maintained at -91 kPa in each cycle, verifying entire sealing and stable picking.

To check the scalability of the developed gripper, the gripper is assumed to be scaled up n times in all directions. The spring constant of the outer spring, which is a major design parameter, follows the equation below [26]:

$$k_b = Gt^4/64N_aR_s^3 \tag{16}$$

where G is the shear modulus of the spring wire material and N_a is the number of active coils. The spring constant increases n times because the wire diameter (t) and radius (R_s) of the spring increase by a factor of n. The gripper' s deployment ratio will be maintained whereas the picking force will increase in proportion to n^2 because both the restoring force of the spring (k_bL) and the compressing force (ΔPA_b) due to the pressure difference increases n^2 times. As a result, by scaling up the proposed gripper, the gripper can exert a stronger picking force while maintaining the same deployment ratio. In dynamic situations, the acceleration and picking speed is expected to decrease since the mass of the spring increases by n^3 times, while the restoring force and compression force increase by n^2 times.

V. Demonstrations

To verify the feasibility of the proposed gripper, five demonstrations on the gripper were conducted. The gripper was able to pick objects of different heights from the same picking height (Fig. 10(a)), eliminating the need for depth sensing to pick up

objects of different heights. Bin picking of transparent objects is challenging, because vision systems suffer from large depth and tilt errors due to the transparency of objects. The gripper solves the bin-picking of transparent dishes by conforming its body to distant and tilted dishes (Fig. 10(b)).

Further extensions of the gripper allow the gripper to not only pick up objects against depth and tilt errors but also conduct versatile tasks. By extending the gripper in parallel using multiple grippers, the gripper can pick multiple objects at different heights simultaneously, enabling depalletizing despite the unmatched number of grippers (three) and objects in each layer (four by four) (Fig. 10(c)). In addition, the extended version of the gripper (140 mm stroke) can penetrate a narrow, deep space that cannot be reached by a manipulator, enabling warehouse picking in occluded environments (Fig. 10(d)). Finally, the proposed gripper with 79 mm stroke was applied to catch a falling balloon at a speed of 1.02 m/s at a distance of 50.1 mm, demonstrating the possibility of dynamic grasping (Fig. 10(e)).

VI. Conclusion

Our study proposed a longitudinally deployable and initially compact compliant suction gripper that reliably picks objects over wide depth and tilt error ranges. Without additional contact sensing, the proposed gripper can pick objects at various distances and orientations by utilizing a compliant body to conform to the object within the range of deployment. We proposed a gripper body and pneumatic circuit design that enable reliable picking, overcoming depth and tilt errors; the picking by the proposed gripper according to the depth error was analyzed using two analytical models and experimentally validated. In addition, picking angle range, maximum picking force, picking speed, and picking reliability were experimentally measured. The feasibility of picking with depth and tilt errors was verified through two demonstrations and three additional demonstrations were suggested.

Future work may include analytical investigations on picking speed to optimize the gripper for dynamically grasping moving objects. Further parametric studies on the thickness or material of the film enclosing the spring would improve the gripper to be resistant to scratches from the external environment. The characteristics of the proposed gripper for robustly picking objects at various distances and angles with high speed are expected to be advantageous for mobile platforms such as drones, where the relative position of the gripper and object dynamically changes. Therefore, we expect the technology to be beneficial not only in static environments with large vision sensing errors but also in dynamic situations.

References

[1] H. Pham and Q. C. Pham, "Critically fast pick-and-place with suction cups," in *Proc. IEEE Int. Conf. Robot. Automat.*, 2019, pp. 3045–3051.

[2] E. Papadakis, F. Raptopoulos, M. Koskinopoulou, and M. Maniadakis, "On the use of vacuum technology for applied robotic systems," in *Proc. IEEE 6th Int. Conf. Mechatron. Robot. Eng.*, 2020, pp. 73–77, 2020.

[3] V. Mueller, R. Behrens, and N. Elkmann, "A new multi-modal approach towards reliable bin-picking application," in *Proc. IEEE 47th Int. Symp. Robot.*, vol. 2016, pp. 473–479, 2016.

[4] M. Schwarz et al., "NimbRo picking: Versatile part handling for warehouse automation," in *Proc. IEEE Int. Conf. Robot. Automat.*, 2017, pp. 3032–3039.

[5] S. Sajjan et al., "Clear grasp: 3D shape estimation of transparent objects for manipulation," in *Proc. IEEE Int. Conf. Robot. Automat.*, 2020, pp. 3634–3642.

[6] K. Kim and H. Shim, "Robust approach to reconstructing transparent objects using a time-of-flight depth camera," *Opt. Exp.*, vol. 25, no. 3, 2017, Art. no. 2666.

[7] E.-T. Baek, H.-J. Yang, S.-H. Kim, G. Lee, and H. Jeong, "Distance error correction in time-of-flight cameras using asynchronous integration time," *Sensors*, vol. 20, no. 4, 2020, Art. no. 1156.

[8] C. Y. Chai, Y. P. Wu, and S. L. Tsao, "Deep depth fusion for black, transparent, reflective and texture-less objects," in *Proc. IEEE Int. Conf. Robot. Automat.*, 2020, pp. 6766–6772.

[9] Y. Piao, Z. Rong, M. Zhang, W. Ren, and H. Lu, "A2dele: Adaptive and attentive depth distiller for efficient RGB-D salient object detection," in *Proc. IEEE Comput. Soc. Conf. Comput. Vis. Pattern Recognit.*, vol. 2, 2020, pp. 9057–9066.

[10] S. Aoyagi, M. Suzuki, T. Morita, T. Takahashi, and H. Takise, "Bellows suction cup equipped with force sensing ability by direct coating thin-film resistor for vacuum type robotic hand," *IEEE/ASME Trans. Mechatron.*, vol. 25, no. 5, pp. 2501–2512, Oct. 2020.

[11] S. Baek and D. O. Kim, "Predictive process adjustment by detecting system status of vacuum gripper in real time during pick-up operations," *Processes*, vol. 9, no. 4, 2021, Art. no. 634.

[12] S. Liu, W. Dong, Z. Ma, and X. Sheng, "Adaptive aerial grasping and perching with dual elasticity combined suction cup," *IEEE Robot. Automat. Lett.*, vol. 5, no. 3, pp. 4766–4773, Jul. 2020.

[13] Y. Cui, S. Schuon, S. Thrun, D. Stricker, and C. Theobalt, "Algorithms for 3D shape scanning with a depth camera," *IEEE Trans. Pattern Anal. Mach. Intell.*, vol. 35, no. 5, pp. 1039–1050, May 2013.

[14] C. C. Chang, K. C. Shih, H. C. Ting, and Y. S. Su, "Utilizing machine learning to improve the distance information from depth camera," in *Proc. IEEE 3rd Eurasia Conf. IOT, Commun. Eng.*, 2021, pp. 405–408.

[15] S. Doi, H. Koga, T. Seki, and Y. Okuno, "Novel proximity sensor for realizing tactile sense in suction cups," in *Proc. IEEE Int. Conf. Robot. Automat.*, 2020, pp. 638–643.

[16] M. Sitti, "Physical intelligence as a new paradigm," *Extreme Mechanics Lett.*, vol. 46, 2021, Art. no. 101340.

[17] C. Laschi, B. Mazzolai, and M. Cianchetti, "Soft robotics: Technologies and systems pushing the boundaries of robot abilities," *Sci. Robot.*, vol. 1, no. 1, pp. 1–12, 2016.

[18] S. Li et al., "A vacuum-driven origami 'Magic-ball' soft gripper," in *Proc. IEEE Int. Conf. Robot. Automat.*, 2019, pp. 7401–7408.

[19] J. Zhou, S. Chen, and Z. Wang, "A soft-robotic gripper with enhanced object adaptation and grasping reliability," *IEEE Robot. Automat. Lett.*, vol. 2, no. 4, pp. 2287–2293, Oct. 2017.

[20] P. E. Pounds, D. R. Bersak, and A. M. Dollar, "Practical aerial grasping of unstructured objects," in *Proc. IEEE Conf. Technol. Practical Robot Appl.*, 2011, pp. 99–104.

[21] F. Angelini, C. Petrocelli, M. G. Catalano, M. Garabini, G. Grioli, and A. Bicchi, "SoftHandler: An integrated soft robotic system for handling heterogeneous objects," *IEEE Robot. Automat. Mag.*, vol. 27, no. 3, pp. 55–72, Sep. 2020.

[22] D. Pascoe, "Vacuum pick-up cylinders," fluidpowerjournal.com. Accessed: Sep. 7, 2022. [Online]. Available: https://fluidpowerjournal.com/vacuum-pick-up-cylinders/

[23] T. McCulloch and D. Herath, "Towards a universal gripper - on the use of suction in the context of the amazon robotic challenge," *Australas. Conf. Robot. Automat.*, 2016, pp. 153–160.

[24] F. M. White, *Fluid Mechanics*, 7th ed. New York, NY, USA: Mc Graw Hill, 2011.

[25] J. G. Lee and H. Rodrigue, "Origami-based vacuum pneumatic artificial muscles with large contraction ratios," *Soft Robot.*, vol. 6, no. 1, pp. 109–117, 2019.

[26] E. Rodriguez, M. Paredes, and M. Sartor, "Analytical behavior law for a constant pitch conical compression spring," *J. Mech. Des.*, vol. 128, no. 6, pp. 1352–1356, 2005.